Siddiqui, T., Yamazaki, Y., Stolle, C., Lühr, H., Matzka, J., Maute, A., Pedatella, N. (2018): Dependence of lunar tide of the equatorial electrojet on the winter-time polar vortex, solar flux and QBO. - *Geophysical Research Letters*, *45*, 9, pp. 3801—3810.

DOI: http://doi.org/10.1029/2018GL077510

Geophysical Research Letters

RESEARCH LETTER
10.1029/2018GL077510

Key Points:
- Lunar tide of the equatorial electrojet during SSWs has been studied using composite analysis
- Larger lunar tidal enhancements are observed during vortex-split SSWs than vortex-displaced SSWs
- Evidence of modulation of lunar tide by the QBO phase is seen during SSWs

Supporting Information:
- Supporting Information S1
- Data Set S1

Correspondence to:
T. A. Siddiqui,
tarique@ucar.edu

Citation:
Siddiqui, T. A., Yamazaki, Y., Stolle, C., Lühr, H., Matzka, J., Maute, A., & Pedatella, N. (2018). Dependence of lunar tide of the equatorial electrojet on the wintertime polar vortex, solar flux, and QBO. *Geophysical Research Letters*, *45*, 3801–3810. https://doi.org/10.1029/2018GL077510

Received 7 FEB 2018
Accepted 5 APR 2018
Accepted article online 19 APR 2018
Published online 7 MAY 2018

Dependence of Lunar Tide of the Equatorial Electrojet on the Wintertime Polar Vortex, Solar Flux, and QBO

T. A. Siddiqui[1,2], Y. Yamazaki[2], C. Stolle[2,3], H. Lühr[2], J. Matzka[2], A. Maute[1], and N. Pedatella[1]

[1]High Altitude Observatory, National Center for Atmospheric Research, Boulder, CO, USA, [2]GFZ German Research Centre for Geosciences, Potsdam, Germany, [3]Faculty of Science, University of Potsdam, Potsdam, Germany

Abstract The lower atmospheric forcing effects on the ionosphere are particularly evident during extreme meteorological events known as sudden stratospheric warmings (SSWs). During SSWs, the polar stratosphere and ionosphere, two distant atmospheric regions, are coupled through the SSW-induced modulation of atmospheric migrating and nonmigrating tides. The changes in the migrating semidiurnal solar and lunar tides are the major source of ionospheric variabilities during SSWs. In this study, we use 55 years of ground-magnetometer observations to investigate the composite characteristics of the lunar tide of the equatorial electrojet (EEJ) during SSWs. These long-term observations allow us to capture the EEJ lunar tidal response to the SSWs in a statistical sense. Further, we examine the influence of solar flux conditions and the phases of quasi-biennial oscillation (QBO) on the lunar tide and find that the QBO phases and solar flux conditions modulate the EEJ lunar tidal response during SSWs in a similar way as they modulate the wintertime Arctic polar vortex. This work provides first evidence of modulation of the EEJ lunar tide due to QBO.

Plain Language Summary This study focuses on the vertical coupling between the polar stratosphere and equatorial ionosphere during sudden stratospheric warmings (SSWs). Extreme meteorological events such as SSWs induce variabilities in the ionosphere by modulating the atmospheric migrating and nonmigrating tides, and these variabilities can be comparable to a moderate geomagnetic storm. Observations and modeling studies have found that the changes in the migrating semidiurnal solar and lunar tides are a major source of ionospheric variabilities during SSWs. The equatorial electrojet (EEJ) is a narrow ribbon of current flowing over the dip equator in the ionosphere and is particularly sensitive to tidal changes. Long-term ground-magnetometer recordings have been used in this study to estimate the variations induced in EEJ during SSWs due to the lunar semidiurnal tide in a statistical sense. The wintertime Arctic polar vortex and the occurrence of SSWs are modulated by solar flux conditions and the phases of quasi-biennial oscillation. In this work, we find the first evidence of lunar tidal modulation of EEJ due to quasi-biennial oscillation during SSWs. Our findings will be useful in providing improved predictions of ionospheric variations due to SSWs. The aeronomy community will be the most impacted by this paper.

1. Introduction

Sudden stratospheric warmings (SSWs) are large-scale wintertime meteorological events usually occurring in the Northern Hemisphere. During SSWs, the stratospheric polar temperature increases by several tens of degrees in a few days and the westerly zonal mean zonal winds (ZMZWs) decelerate or in some cases may even reverse their direction (e.g., Scherhag, 1952). SSWs can lead to displacement or splitting of the polar vortex, and depending on the nature of the polar vortex breakdown, SSWs can be classified as vortex split or vortex displaced. The displacement and splitting of the polar vortex are predominantly associated with forcing of the planetary wave (PW) with zonal wavenumbers 1 and 2, respectively (e.g., Andrews et al., 1987). The widely accepted mechanism responsible for SSWs is the amplification of quasi-stationary PWs and its nonlinear interaction with the stratospheric zonal mean flow(e.g., Matsuno, 1971). The dynamical effects associated with SSWs are not just confined to the polar latitudes but also extend into the middle and equatorial latitudes (e.g., Goncharenko & Zhang, 2008; Goncharenko et al., 2010; Julian & Labitzke, 1965; H.-L. Liu & Roble, 2002).

The modulation of equatorial ionosphere during SSWs as a result of enhanced atmospheric solar and lunar semidiurnal tides has been widely reported in recent years (e.g., Chau et al., 2012, and references therein).

The atmospheric lunar tide is mainly generated in the lower atmosphere and then propagates to ionospheric heights, where the dynamo action of the winds associated with these tides drive ionospheric variations (e.g., Matsushita & Xu, 1984). The propagating lunar tide is sensitive to the background wind and temperature conditions, and its enhancement during SSWs is mainly associated with the dynamical changes in the middle atmosphere that accompany these events (e.g., Forbes & Zhang, 2012). Many recent studies have focused on the lunar tidal amplification during SSWs in the daytime ionospheric current flow known as the equatorial electrojet (EEJ) from ground-magnetometer measurements (e.g., Fejer et al., 2010; Siddiqui et al., 2015; Yamazaki et al., 2012). However, the specific characteristics of lunar tidal enhancements during vortex-split and vortex-displaced SSWs have never been studied. Here we utilize the data from the Huancayo (12.1°S, 75.2°W) magnetic observatory in Peru to study the composite lunar tidal characteristics in EEJ during vortex-split and vortex-displaced SSWs. Additionally, we investigate the dependence of the EEJ lunar tide on the phases of quasi-biennial oscillation (QBO). We also examine if the wintertime variability induced in the polar stratosphere due to QBO phases and solar flux conditions as reported by Labitzke (1987) and Labitzke et al. (2006) has an effect on the lunar tide of the EEJ during SSWs.

After the recent digitization of handwritten magnetic recordings at Huancayo from 1967 to 1985 (Matzka et al., 2017), a continuous set of data from 1958 to 2013 are available for the purpose of this study, which makes it possible to investigate the dependence of the ionospheric lunar tidal response on the characteristic of the polar vortex, solar flux conditions, and QBO phases. In the following section we describe the data used in this study. Section 3 presents the methodology followed by the results in section 4. In section 5, the results are discussed and conclusions are summarized.

2. Data

Hourly mean values of the horizontal (H) component ground-magnetometer recordings at the Huancayo observatory are downloaded for the years 1958–2013 from the website of World Data Centre for Geomagnetism, Edinburgh. The missing data between 1967 and 1985, which are unavailable at the World Data Centre, are filled by including the newly digitized recordings. The resulting data set, used for this study, is published by GFZ Data Services (Matzka et al., 2018) and is available as supporting information to this paper.

The central dates of major vortex-displaced and vortex-split SSWs between 1958 and 2013 are taken from Charlton and Polvani (2007) and C. Liu et al. (2014). Diurnal mean values of zonal wind between 60°N and 90°N and 1000- to 10-hPa pressure levels are calculated from the National Centers for Environmental Prediction-National Center for Atmospheric Research reanalysis data sets (Kalnay et al., 1996). The monthly equatorial zonal winds, which characterize the QBO, are downloaded for the 50- and 40-hPa pressure levels from the website of Institute of Meteorology, Frei Universität, Berlin. The monthly mean values of the equatorial zonal winds from the 50- to 40-hPa pressure levels are calculated and are used to define the easterly and the westerly phases of QBO (e.g., Labitzke et al., 2006; Naujokat, 1986). The easterly and westerly phases of QBO are henceforth denoted as eQBO and wQBO, respectively.

3. Methods

Regular daily variations with period and subperiods of a lunar day are found in ground-magnetic records and are termed as geomagnetic lunar (L) daily variations. The dominant component of L is the semidiurnal variation (12.42 solar hours), which displays a semimonthly variation (14.77 days) at a fixed local time (LT). The semidiurnal lunar tide (M_2) dominates the lunar tidal effects in the geomagnetic field, while the contributions from lunar elliptic semidiurnal (N_2) and lunar diurnal (O_1) tides are minor (Stening, 1975). The lunar tidal modulation of the EEJ amounts to about 15% of the EEJ intensity on normal days (e.g., Lühr et al., 2012), but the modulation can increase by up to 4–5 times during certain days (e.g., Bartels & Johnston, 1940). One of the causes for these large lunar tidal enhancements in the EEJ is attributed to the modified lunar tidal propagation conditions in the atmosphere during SSWs (e.g., Vineeth et al., 2009). It is also important to note that the lunar tide of the EEJ shows a seasonal enhancement during the December solstice at all longitudes (e.g., Yamazaki et al., 2017) irrespective of an SSW event. However, the EEJ lunar tidal amplitude can increase to a much larger amount during SSWs in comparison to its seasonal enhancement (e.g., Park et al., 2012).

In this study, the semimonthly lunar tidal modulation of the EEJ is estimated using the single observatory method described in detail in Siddiqui et al. (2015). Briefly, the total magnetic field variation at the dip

Table 1
List of the Major SSW Events Recorded Between 1958 and 2013

No.	Central date	Vortex type	QBO phase	$F_{10.7}$ (s.f.u)	Peak lunar tidal power (nT^2)	Peak ZMZW anomalies at 10 hPa (m/s)
1	30 Jan 1958	Split	West	243.45	1,476.8	−19.1
2	30 Nov 1958	Displaced	East	204.58	443.6	−8.2
3	16 Jan 1960	Displaced	West	195.20	710.1	−7.1
4	23 Mar 1965	Split	West	73.01	319.2	−1.8
5	8 Dec 1965	Displaced	East	74.06	483.7	−12.2
6	24 Feb 1966	Split	East	82.15	1,052.9	−13.7
7	8 Jan 1968	Split	West	183.06	912.6	−9.9
8	27 Nov 1968	Displaced	East	135.51	773.9	−8.2
9	13 Mar 1969	Displaced	East	170.62	314.6	−5.1
10	2 Jan 1970	Displaced	West	153.48	562.9	−10.9
11	17 Jan 1971	Split	East	157.38	892.2	−12.0
12	20 Mar 1971	Displaced	East	110.79	330.5	−6.7
13	2 Feb 1973	Split	East	96.25	1,530.1	−12.3
14	22 Feb 1979	Split	West	199.11	907.2	−16.3
15	29 Feb 1980	Displaced	East	195.06	485.8	−16.2
16	4 Dec 1981	Displaced	East	201.36	258.1	−5.8
17	24 Feb 1984	Displaced	East	137.17	821.8	−13.4
18	2 Jan 1985	Split	East	72.08	1,569.6	−9.9
19	23 Jan 1987	Displaced	East	70.18	992.6	−14.5
20	8 Dec 1987	Split	West	91.45	590.4	−19.5
21	14 Mar 1988	Split	West	113.83	501.6	−9.1
22	22 Feb 1989	Split	West	216.95	672.3	−7.8
23	15 Dec 1998	Displaced	East	145.46	938.5	−15.6
24	25 Feb 1999	Split	East	138.59	407.9	−14.8
25	20 Mar 2000	Displaced	West	206.11	288.6	−0.8
26	11 Feb 2001	Split	East	143.10	807.5	−11.4
27	2 Jan 2002	Displaced	East	220.05	651.9	−4.4
28	18 Jan 2003	Split	West	139.53	1,860.1	−6.4
29	7 Jan 2004	Displaced	East	109.86	1,128.2	−12.1
30	21 Jan 2006	Displaced	East	80.46	1,741.4	−22.2
31	24 Feb 2007	Displaced	West	75.30	409.5	−18.3
32	22 Feb 2008	Displaced	East	69.38	1,422.1	−17.5
33	24 Jan 2009	Split	West	67.62	1,529.8	−14.9
34	9 Feb 2010	Split	East	82.77	1,131.9	−13.8
35	7 Jan 2013	Split	East	122.62	1,539.1	−19.3

Note. SSW = sudden stratospheric warming; QBO = quasi-biennial oscillation; ZMZW = zonal mean zonal wind.

equator is composed of the Earth's main (core) field, the field due to the magnetospheric ring current, the field due to solar quiet (Sq) current system, and the EEJ. The hourly *H* component recordings are first subtracted with the Dst values to minimize the disturbance field due to the ring current. We make use of the nighttime values between 23 and 03 LT during the five international quiet days (IQDs), which are released every month by GFZ Potsdam, to determine a mean monthly estimate of the Earth's main field. This baseline value is then subtracted from the hourly magnetic recordings to remove the estimated Earth's main field component.

The daily variation, ΔH, is defined as the deviation from this baseline value. ΔH shows a dependence on solar activity due to varying ionospheric conductivity (e.g., Alken & Maus, 2007). Daily solar flux ($F_{10.7}$) values

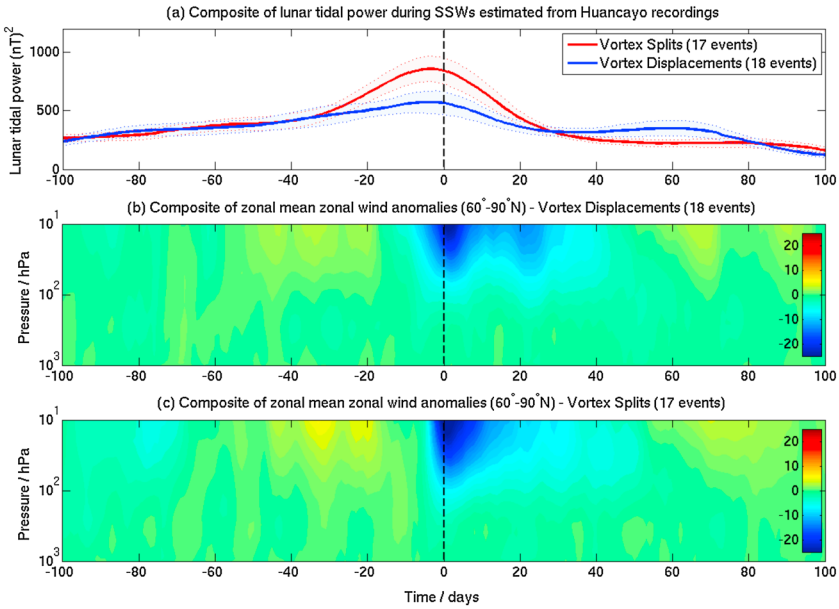

Figure 1. (a) Composites of the lunar tidal power from Huancayo recordings for vortex-split (red line) and vortex-displaced (blue line) events. The shaded regions represent the 1 σ uncertainty levels. (b) Composite of the area-weighted zonal mean zonal wind anomaly (m/s) between 60°N and 90°N for vortex-displaced sudden stratospheric warmings (SSWs). (c) Same as (b) but for vortex-split events. The dashed black vertical lines indicate the central day of the composites.

(Tapping, 2013) are used for minimizing the solar cycle signal in the EEJ, and ΔH is normalized to a solar flux level of 150 s.f.u (e.g., Park et al., 2012; Siddiqui et al., 2015). The normalized ΔH is arranged into bins of 1 day by 1 hr in LT. The geomagnetic solar variation (S) is the dominant variation in ΔH, and it is estimated and removed by using the following method. For each day, a 59-day ($\sim 14.77 \times 4$) centered sliding window is selected and the mean values for each LT hour between 07:00 and 17:00 LT are calculated and subtracted from the ΔH values within the window. The residuals ($\Delta H - S$) are used to compute the lunar tidal amplitude and phase for each considered LTs using the fast Fourier transform (Siddiqui et al., 2015). The amplitude obtained for each LT is then normalized for the expected diurnal variation of the ionospheric conductivity, as described by Lühr et al. (2008). A mean semimonthly lunar wave for each sliding window is obtained by calculating the mean of the normalized amplitudes for all the considered LTs and then assigned to its central day.

4. Results

4.1. Composites of Lunar Tidal Power for Vortex-Split and Vortex-Displaced SSWs

The central date of SSWs recorded between 1958 and 2013 and their classification into vortex split and vortex displaced are listed in Table 1. The corresponding QBO phases, monthly solar flux values (s.f.u), peak lunar tidal power (nT^2), and peak ZMZW anomalies (m/s) at 10 hPa during each of the SSW events are also listed in Table 1. The central dates are based on the earliest reversal of the ZMZWs at 60°N and 10 hPa during the northern winter months. The total number of split and displaced events recorded during this period are 17 and 18, respectively. Figure 1a presents the composite of the lunar tidal power estimated from Huancayo recordings for vortex-displaced (blue line) and vortex-split (red line) SSWs. We have used an interval of 100 days before and after the central date for the composite analysis. The shaded regions represent the standard error (σ) of the mean lunar tidal power, and the upper and lower boundaries denote the 1 σ uncertainty level.

Following Charlton and Polvani (2007), the area-weighted mean polar cap (60°N–90°N) zonal wind is calculated from the reanalysis data set and on subtraction from its climatology values the anomalies are obtained. Figures 1b and 1c present the evolution of area-weighted mean polar cap (60°N–90°N) ZMZW anomaly as a function of pressure and time for vortex-displaced (Figure 1b) and vortex-split (Figure 1c) SSWs. From Figure 1a, it is observed that the lunar tidal power estimated during vortex-split SSWs is ~50% greater compared to the vortex-displaced SSWs on the central SSW date. The lunar tidal peak is recorded 4 days before the central SSW date for both the split and displaced SSWs, and the peak values are 858.1 and 564.1 nT^2, respec-

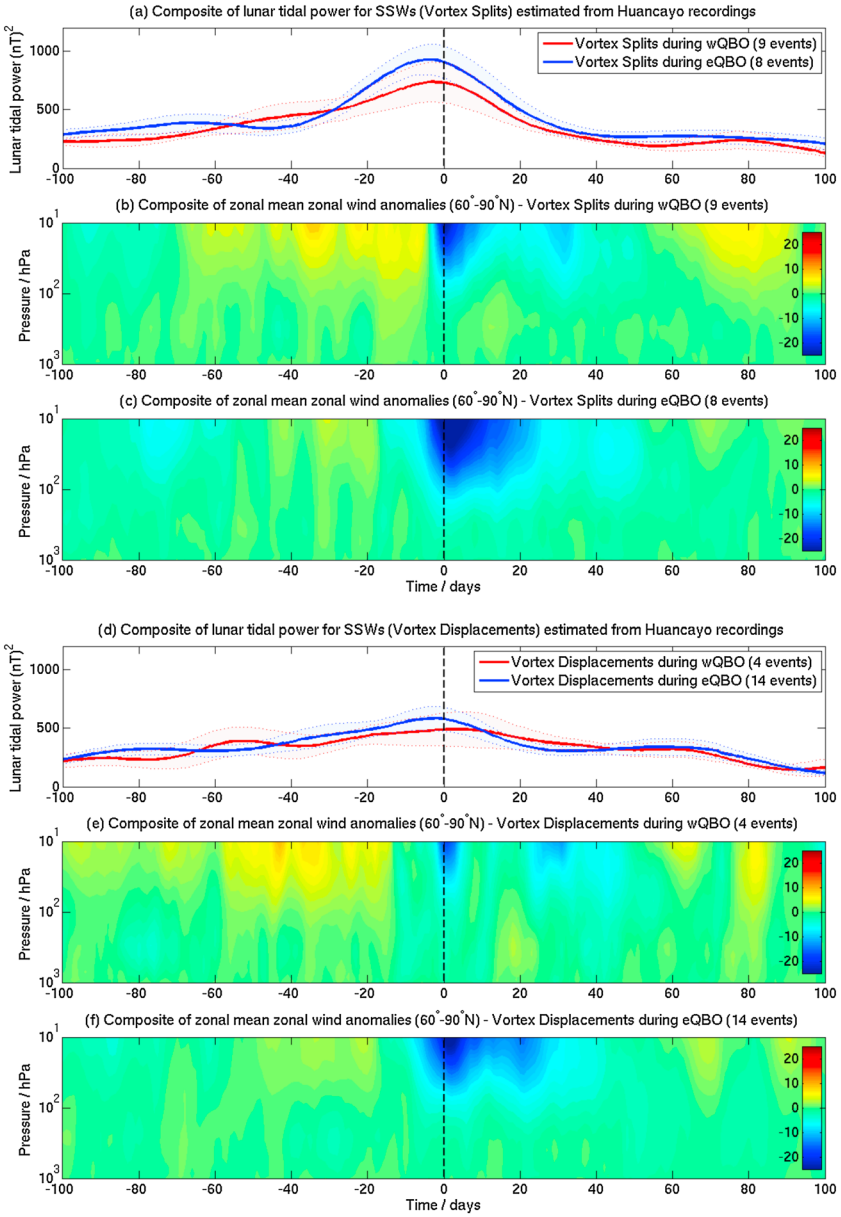

Figure 2. (a) Composites of the lunar tidal power from Huancayo recordings for vortex-split SSWs during wQBO (red line) and during eQBO (blue line). The shaded regions represent the 1 σ uncertainty levels. (b) Composite of the area-weighted ZMZW anomaly (m/s) between 60°N and 90°N for vortex-split SSWs during wQBO. (c) Same as (b) but for vortex-split SSWs during eQBO. (d–f) Same as (a)–(c) except for vortex-displaced SSWs. The dashed black vertical lines indicate the central day of the composites. SSW = sudden stratospheric warming; ZMZW = zonal mean zonal wind; wQBO = westerly quasi-biennial oscillation; eQBO = easterly quasi-biennial oscillation.

tively. In both cases, the lunar tidal power shows a sudden enhancement around the central SSW date before reducing to pre-SSW levels. The lunar tidal power decreases more rapidly in the decay phase of vortex-spilt SSWs, before similar power values are reached in both cases at around 90 days after the central SSW date.

In Figures 1b and 1c, a large negative ZMZW anomaly, indicating the vortex deceleration, is clearly seen around the central SSW date. The transition of the ZMZW anomaly from positive to negative is more sudden in case of vortex-split SSWs. The ZMZW anomaly reaches a value of −24.1 m/s for vortex displaced and −27.3 m/s for vortex split on the central SSW date at the 10-hPa level, which suggests that the intensity of vortex deceleration is stronger in case of vortex-split SSWs. The ZMZW anomalies in Figure 1 are consistent with the results of Charlton and Polvani (2007). The lunar tidal enhancements in Figure 1a can be clearly seen to coincide with

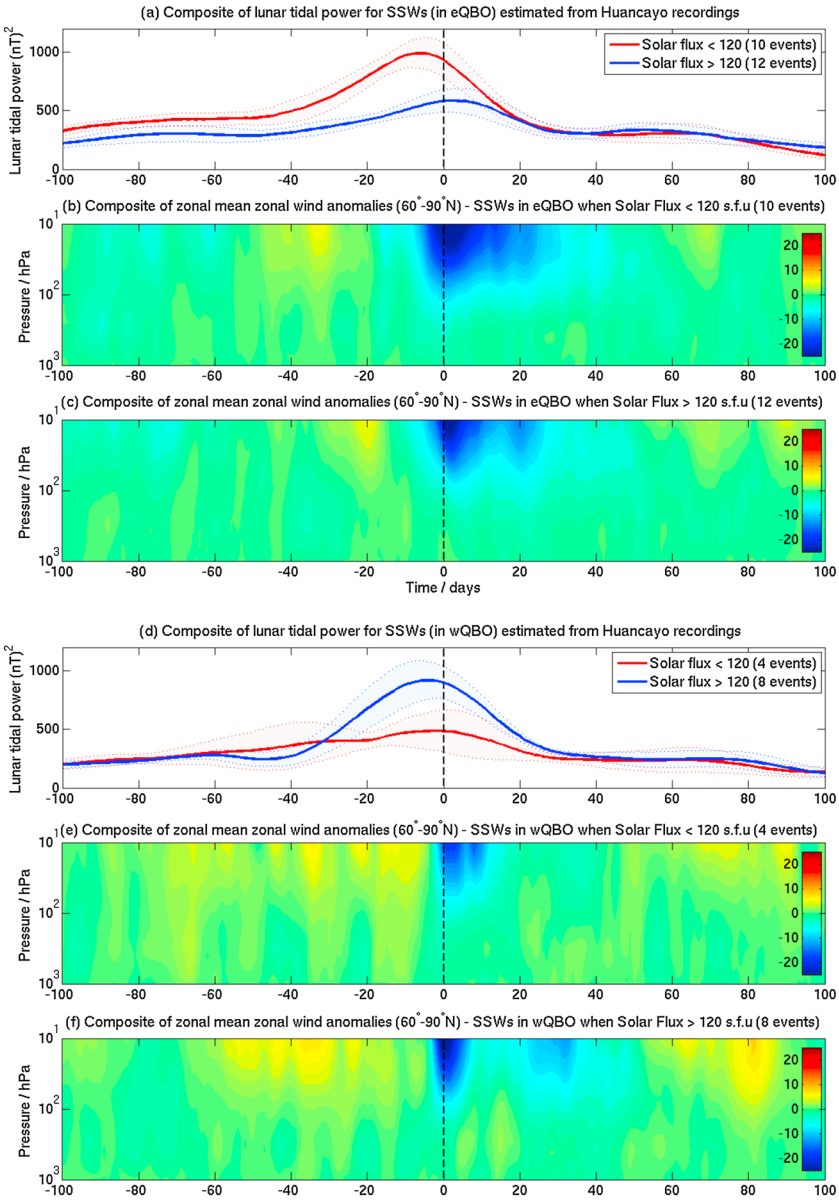

Figure 3. (a) Composite of the lunar tidal power from Huancayo recordings for SSWs in eQBO. The red (blue) line shows the mean lunar tidal power when solar flux values are < (>) 120 s.f.u. The shaded regions represent the 1 σ uncertainty levels. (b) Composite of the area-weighted ZMZW anomaly (m/s) between 60°N and 90°N for SSWs that are recorded during eQBO when the solar flux values < 120 s.f.u. (c) Same as (b) but for SSWs recorded during eQBO when the solar flux values > 120 s.f.u. (d–f) Same as (a)–(c) except for SSWs in wQBO. The dashed vertical black lines indicate the central day of the composites. SSW = sudden stratospheric warming; ZMZW = zonal mean zonal wind; wQBO = westerly quasi-biennial oscillation; eQBO = easterly quasi-biennial oscillation.

the strength of ZMZW anomalies as larger enhancements are recorded when the negative ZMZW anomalies are stronger.

4.2. Composites of Lunar Tidal Power for Vortex-Split and Vortex-Displaced SSWs During Different QBO Phases

In this section, the vortex-split and vortex-displaced SSWs listed in Table 1 are further sorted according to their respective QBO phases and we investigate if the lunar tidal enhancements are modulated by the QBO phases during these vortex-split and vortex-displaced SSWs. The number of vortex-split events, which occurred during the eQBO and wQBO, are 8 and 9, respectively. Figure 2a presents the composite of the lunar tidal power for vortex splits in the wQBO (red line) and eQBO (blue line). Figures 2b and 2c present the polar cap ZMZW

anomalies for vortex splits during the wQBO and eQBO, respectively. It is observed that the lunar tidal power for vortex splits is ∼ 24% larger in the eQBO than in the wQBO on the central SSW date. Peak lunar power value of 926.9 nT^2 (734.3 nT^2) is recorded 4 (2) days before the central date in the eQBO (wQBO). In case of vortex splits in the wQBO, the positive to negative change in the ZMZW anomalies (Figure 2b) starts later and its intensity is also weaker around the central SSW date than in the eQBO (Figure 2c). Similar to Figure 1a, the lunar tidal power values in Figure 2a can be seen to correspond with the strength of negative ZMZW anomalies in Figures 2b and 2c.

The number of vortex-displaced events, which occurred during the eQBO and wQBO, are 14 and 4, respectively. It is interesting to note that the vortex-displaced events are clearly more favored to occur in the eQBO than wQBO. Figures 2d–2f present the lunar tidal power, the polar cap ZMZW anomalies for vortex splits during the wQBO and eQBO, respectively. Like in Figure 2a, the lunar tidal composite for vortex-displaced SSWs in the wQBO (eQBO) in Figure 2d is denoted by red (blue) line. Due to a relatively fewer number of vortex-displaced events in the wQBO, the standard error is larger around the central SSW date compared to the eQBO. Peak lunar power value of 583.8 nT^2 (480.9 nT^2) is recorded 2 (3) days before (after) the central date in the eQBO (wQBO). From Figures 2e and 2f, it can be observed that the negative ZMZWs are stronger for the vortex-displaced SSWs in the eQBO than wQBO, which corresponds with the larger lunar tidal enhancements in the eQBO.

4.3. Composite of Lunar Tidal Power During Different QBO Phases and Solar Flux Conditions

Labitzke (1987) and Labitzke and Loon (1988) detected the QBO and the 11-year solar cycle influence on the polar vortex by stratifying the North Pole temperature and geopotential height based on their respective QBO phases. They also found that there is a tendency of SSWs recorded in the eQBO to occur during solar minima and those recorded in the wQBO to occur during solar maxima. In this section, we investigate whether the influence of QBO and solar cycle variability on the winter polar stratosphere has an effect on the lunar tides of the EEJ during SSWs.

The SSWs listed in Table 1 have been first stratified according to their QBO phases. A monthly solar flux (SF) value of 120 s.f.u has been chosen to sort the SSWs into solar minimum and maximum levels. In eQBO, a total of 10 SSWs are recorded when the SF values < 120 s.f.u (Smin) and 12 when the SF values > 120 s.f.u (Smax). Composites of the lunar tidal power and the ZMZW anomalies during the eQBO and wQBO are presented for Smax and Smin conditions in Figure 3. Figure 3a shows the lunar tidal power under the eQBO/Smin (red line) and eQBO/Smax (blue line) conditions. The peak in lunar tidal power equals 989.8 nT^2 (586.4 nT^2) and is seen 6 (3) days before (after) the central SSW date under Smin (Smax) conditions. The lunar tidal power, in general, remains greater for the entire duration before the central SSW date under Smin conditions. Around 20 days after the central date, a parity in the lunar tidal power is achieved in both cases, which continues for the remaining period of analysis. In Figures 3b and 3c, the intensity of the ZMZW anomalies around the central SSW date can be observed to differ with the SF conditions. The positive to negative change in the ZMZW anomalies under Smin conditions starts earlier, and larger anomaly values are recorded compared to Smax conditions. This difference is also seen in the lunar tidal enhancements, shown in Figure 3a, as larger enhancements are observed in eQBO during Smin conditions than Smax conditions.

In wQBO, a total of eight SSWs are recorded when SF > 120 s.f.u and five SSWs when SF < 120 s.f.u. The wQBO and Smin case includes the 2009 SSW event (Labitzke & Kunze, 2013) during which the lunar tidal power was observed to be anomalously larger (see Table 1) compared to the four other SSWs in this case. This SSW event has therefore been treated as an outlier and not been included in the composite analysis. Figure 3d shows the lunar tidal power under the wQBO/Smin (red line) and wQBO/Smax (blue line) conditions. The peak lunar tidal power is estimated 4 (3) days before the central SSW date and equals 917.9 nT^2 (434.1 nT^2) under Smin (Smax) conditions. Figures 3e and 3f present the ZMZW anomalies during the wQBO/Smin and wQBO/Smax conditions, respectively. Around the central date, the intensity of the ZMZW anomalies shows a noticeable difference with a larger negative anomaly being observed in wQBO/Smax than wQBO/Smin and this observation is opposite in the eQBO case. Larger lunar tidal enhancements (Figure 3d) are also recorded when the anomalies are seen to be larger under wQBO/Smin.

5. Discussion and Conclusions

Charlton and Polvani (2007) highlighted the difference in the vertical profile of the polar cap temperature and ZMZW anomalies in the troposphere and stratosphere through composite analysis prior to, during, and

after the occurrence of vortex-split and vortex-displaced SSWs. The intensity of PW forcing, estimated through meridional heat flux anomalies, also differed with larger anomalies being recorded in the case of vortex-split SSWs. It is not unrealistic to assume that these dynamical differences during vortex-split and vortex-displaced SSWs are not just limited to the troposphere and stratosphere but also extend into the mesosphere and lower thermosphere region. Since numerical studies have already demonstrated that the lunar tide in the mesosphere and lower thermosphere is very sensitive to the state of middle atmosphere (20–80 km) (e.g., Forbes & Zhang, 2012; Stening et al., 1997), it is plausible that the background atmospheric conditions become more favorable for lunar tidal amplification (Figure 1a) due to PW forcing during vortex-split SSWs than vortex-displaced SSWs. We suggest that the differences in the lunar tidal power during vortex-split and vortex-displaced SSWs are mainly due to the variations in the intensity of PW forcing and its associated effects on wind and temperature in the lower and middle atmosphere. The modified atmospheric conditions are responsible for the amplification of the propagating lunar tide. We plan to use the global-scale wave model to test these mechanisms in a future study.

The QBO phase affects the propagation and breaking of the PWs by modulating the position of the zero wind line (e.g., Haynes et al., 1991). The amplified stationary PWs are found to break more poleward during eQBO than wQBO (e.g., Holton & Austin, 1991; McIntyre & Palmer, 1983), which results in the polar vortex becoming more disturbed and warmer during eQBO than wQBO. Holton and Tan (1980) and Labitzke (1982) also reported that more midwinter SSWs occurred in the eQBO than in the wQBO. The analysis of the occurrence rate of SSWs between 1958 and 2013 reveals that while the displaced SSWs do favor the eQBO, the split SSWs do not show such a clear bias. The observations in Figure 2 indicate that the polar vortex, in general, is more disturbed for both vortex-split and vortex-displaced SSWs in eQBO than in wQBO. During wQBO, the PW forcing into the stratosphere is spread over a larger latitudinal width than in eQBO, which results in a lower intensity of breaking PWs in the high-latitude stratosphere and this results in magnitude of negative ZMZW anomalies being smaller. The lunar tidal enhancements in EEJ as seen in Figures 2a and 2d coincide very well with the intensity of these anomalies and we conclude that the QBO modulation of PW forcing is an important factor in deciding the level of lunar tidal enhancement in the EEJ.

Labitzke (1987) reported that under wQBO/Smax conditions, the polar vortex is weaker relative to wQBO/Smin conditions, while an opposite behaviour is seen under eQBO. Camp and Tung (2007) found the wQBO/Smin as the least perturbed state of the polar stratosphere during Arctic winter than eQBO/Smin, wQBO/Smax, and eQBO/Smax. The solar signal in the stratosphere is known to be modulated by QBO (e.g., Labitzke et al., 2006), and on stratifying the lunar tidal enhancements according to the QBO phase (Figure 3) we found that the lunar tidal power in the EEJ during SSWs is getting modulated by the QBO and the solar flux in a similar manner as the Arctic polar vortex. Our observations are consistent with the results of Labitzke et al. (2006) and Camp and Tung (2007). The mechanism by which the interaction of 11-year solar cycle and QBO signals modulate the Arctic polar vortex is not yet fully clear. Gray et al. (2004) proposed a mechanism, which explains why major SSWs under wQBO/Smax and eQBO/Smin, are more frequent and occur earlier. They suggested that the zonal wind anomalies in the equatorial/subtropical upper stratosphere associated with the QBO and 11-year solar cycle reinforce each other during wQBO/Smax and eQBO/Smin conditions and cancel each other out during wQBO/Smin and eQBO/Smax conditions. From our composite results, we find that stronger SSWs are recorded under eQBO/Smin and wQBO/Smax, which offers more favorable conditions for lunar tidal enhancements in EEJ than eQBO/Smax and wQBO/Smin.

Relationship between the QBO and atmospheric tidal variations has been regularly investigated, but the EEJ lunar tidal relation with the QBO has not yet been reported. In this work, we find the first evidence of lunar tide of the EEJ being influenced by the phase of QBO, PW forcing, and solar flux conditions. The lunar tidal enhancements related to these three factors have been analyzed through composite analysis and the conclusions can be summarized as follows:

1. Lunar tidal enhancements in EEJ are larger for vortex-split SSWs than vortex-displaced SSWs.
2. Lunar tidal enhancements in EEJ are larger in eQBO than in wQBO for both vortex-split and vortex-displaced SSWs.
3. Lunar tidal enhancements in EEJ are larger in eQBO (wQBO) under Smin (Smax) conditions than under Smax (Smin) conditions.

Acknowledgments
We thank the Instituto Geofisico del Peru for supporting geomagnetic observatory operations at Huancayo. The $F_{10.7}$ data are obtained from NASA GSFC/SPDF OMNIWeb. The NCEP-NCAR reanalysis data are available at the NOAA/OAR/ESRL website. We are grateful to World Data Centre, Kyoto, for Dst indices. The QBO data are downloaded from Frei Universität, Berlin. International Quiet Days data are available from GFZ Potsdam. C. S., J. M., and H. L. are partly supported by SPP 1788 "Dynamic Earth" of the Deutsche Forschungsgemeinschaft (DFG). The National Center for Atmospheric Research is sponsored by National Science Foundation. T. A. S. and A. M. are supported by NASA grant X13AF77G.

References

Alken, P., & Maus, S. (2007). Spatio-temporal characterization of the equatorial electrojet from CHAMP, Ørsted, and SAC-C satellite magnetic measurements. *Journal of Geophysical Research*, *112*, A09305. https://doi.org/10.1029/2007JA012524

Andrews, D. G., Holton, J. R., & Leovy, C. B. (1987). *Middle atmosphere dynamics* (Vol. 40). San Diego, CA: Academic Press.

Bartels, J., & Johnston, H. F. (1940). Geomagnetic tides in horizontal intensity at Huancayo. *Terrestrial Magnetism and Atmospheric Electricity*, *45*(3), 269–308. https://doi.org/10.1029/TE045i003p00269

Camp, C. D., & Tung, K.-K. (2007). The influence of the solar cycle and QBO on the late-winter stratospheric polar vortex. *Journal of the Atmospheric Sciences*, *64*(4), 1267–1283. https://doi.org/10.1175/JAS3883.1

Charlton, A. J., & Polvani, L. M. (2007). A new look at stratospheric sudden warmings. Part I: Climatology and modeling benchmarks. *Journal of Climate*, *20*(3), 449–469. https://doi.org/10.1175/JCLI3996.1

Chau, J. L., Goncharenko, L. P., Fejer, B. G., & Liu, H.-L. (2012). Equatorial and low latitude ionospheric effects during sudden stratospheric warming events. *Space Science Reviews*, *168*(1), 385–417. https://doi.org/10.1007/s11214-011-9797-5

Fejer, B. G., Olson, M. E., Chau, J. L., Stolle, C., Lühr, H., Goncharenko, L. P., et al. (2010). Lunar-dependent equatorial ionospheric electrodynamic effects during sudden stratospheric warmings. *Journal of Geophysical Research*, *115*, A00G03. https://doi.org/10.1029/2010JA015273

Forbes, J. M., & Zhang, X. (2012). Lunar tide amplification during the January 2009 stratosphere warming event: Observations and theory. *Journal of Geophysical Research*, *117*, A12312. https://doi.org/10.1029/2012JA017963

Goncharenko, L. P., Chau, J. L., Liu, H.-L., & Coster, A. J. (2010). Unexpected connections between the stratosphere and ionosphere. *Geophysical Research Letters*, *37*, L10101. https://doi.org/10.1029/2010GL043125

Gray, L. J., Crooks, S., Pascoe, C., Sparrow, S., & Palmer, M. (2004). Solar and QBO influences on the timing of stratospheric sudden warmings. *Journal of the Atmospheric Sciences*, *61*(23), 2777–2796. https://doi.org/10.1175/JAS-3297.1

Goncharenko, L. P., & Zhang, S.-R. (2008). Ionospheric signatures of sudden stratospheric warming: Ion temperature at middle latitude. *Geophysical Research Letters*, *35*, L21103. https://doi.org/10.1029/2008GL035684

Haynes, P. H., McIntyre, M. E., Shepherd, T. G., Marks, C. J., & Shine, K. P. (1991). On the "downward control" of extratropical diabatic circulations by eddy-induced mean zonal forces. *Journal of the Atmospheric Sciences*, *48*(4), 651–678. https://doi.org/10.1175/1520-0469(1991)048<0651:OTCOED>2.0.CO;2

Holton, J. R., & Austin, J. (1991). The influence of the equatorial QBO on sudden stratospheric warmings. *Journal of the Atmospheric Sciences*, *48*(4), 607–618. https://doi.org/10.1175/1520-0469(1991)048<0607: TIOTEQ>2.0.CO;2

Holton, J. R., & Tan, H.-C. (1980). The influence of the equatorial Quasi-Biennial Oscillation on the global circulation at 50 mb. *Journal of the Atmospheric Sciences*, *37*(10), 2200–2208. https://doi.org/10.1175/1520-0469(1980) 037<2200:TIOTEQ>2.0.CO;2

Julian, P. R., & Labitzke, K. B. (1965). A study of atmospheric energetics during the January-February 1963 stratospheric warming. *Journal of the Atmospheric Sciences*, *22*(6), 597–610. https://doi.org/10.1175/1520-0469(1965)022<0597:ASOAED>2.0.CO;2

Kalnay, E., Kanamitsu, M., Kistler, R., Collins, W., Deaven, D., Gandin, L., et al. (1996). The NCEP/NCAR 40-year reanalysis project. *Bulletin of the American Meteorological Society*, *77*(3), 437–472. https://doi.org/10.1175/1520-0477(1996)077<0437:TNYRP>2.0.CO;2

Labitzke, K. (1982). On the interannual variability of the middle stratosphere during the northern winters. *Journal of the Meteorological Society of Japan, Series. II*, *60*(1), 124–139. https://doi.org/10.2151/jmsj1965.60.1_124

Labitzke, K. (1987). Sunspots, the QBO, and the stratospheric temperature in the north polar region. *Geophysical Research Letters*, *14*(5), 535–537. https://doi.org/10.1029/GL014i005p00535

Labitzke, K., Kunze, M., & Brönnimann, S. (2006). Sunspots, the QBO and the stratosphere in the north polar region—20 years later. *Meteorologische Zeitschrift*, *15*(3), 355–363. https://doi.org/10.1127/0941-2948/2006/0136

Labitzke, K., & Kunze, M. (2013). Interannual variability and trends in the stratosphere, *Climate and Weather of the Sun-Earth System (CAWSES)* (pp. 573–583). Dordrecht, Netherlands: Springer. https://doi.org/10.1007/978-94-007-4348-9_30

Labitzke, K., & Loon, H. V. (1988). Associations between the 11-year solar cycle, the QBO and the atmosphere. Part I: The troposphere and stratosphere in the northern hemisphere in winter. *Journal of Atmospheric and Terrestrial Physics*, *50*(3), 197–206. https://doi.org/10.1016/0021-9169(88)90068-2

Liu, C., Tian, B., Li, K.-F., Manney, G. L., Livesey, N. J., Yung, Y. L., et al. (2014). Northern hemisphere mid-winter vortex-displacement and vortex-split stratospheric sudden warmings: Influence of the Madden-Julian Oscillation and Quasi-Biennial Oscillation. *Journal of Geophysical Research: Atmospheres*, *119*, 12,599–12,620. https://doi.org/10.1002/2014JD021876

Liu, H.-L., & Roble, R. G. (2002). A study of a self-generated stratospheric sudden warming and its mesospheric-lower thermospheric impacts using the coupled TIME-GCM/CCM3. *Journal of Geophysical Research*, *107*(D23), 4695. https://doi.org/10.1029/2001JD001533

Lühr, H., Rother, M., Häusler, K., Alken, P., & Maus, S. (2008). The influence of nonmigrating tides on the longitudinal variation of the equatorial electrojet. *Journal of Geophysical Research*, *113*, A08313. https://doi.org/10.1029/2008JA013064

Lühr, H., Siddiqui, T. A., & Maus, S. (2012). Global characteristics of the lunar tidal modulation of the equatorial electrojet derived from CHAMP observations. *Annales Geophysicae*, *30*(3), 527–536. https://doi.org/10.5194/angeo-30-527-2012

Matsuno, T. (1971). A dynamical model of the stratospheric sudden warming. *Journal of the Atmospheric Sciences*, *28*(8), 1479–1494. https://doi.org/10.1175/1520-0469(1971)028<1479:ADMOTS>2.0.CO; 2

Matzka, J., Lilienkamp, H., Soares, G. B., Rosales, D., Vidal, E., & Siddiqui, T. A. (2018). Hourly mean values of the horizontal component at the geomagnetic observatory Huancayo (HUA), 1958 to 2013. V. 1.*GFZ Data Services*. https://doi.org/10.5880/GFZ.2.3.2018.003

Matzka, J., Siddiqui, T. A., Lilienkamp, H., Stolle, C., & Veliz, O. (2017). Quantifying solar flux and geomagnetic main field influence on the equatorial ionospheric current system at the geomagnetic observatory Huancayo. *Journal of Atmospheric and Solar-Terrestrial Physics*, *163*, 120–125. https://doi.org/10.1016/j.jastp.2017.04.014

Matsushita, S., & Xu, W.-Y. (1984). Seasonal variations of L equivalent current systems. *Journal of Geophysical Research*, *89*(A1), 285–294. https://doi.org/10.1029/JA089iA01p00285

McIntyre, M. E., & Palmer, T. N. (1983). Breaking planetary waves in the stratosphere. *Nature*, *305*, 593–600. https://doi.org/10.1038/305593a0

Naujokat, B. (1986). An update of the observed Quasi-Biennial Oscillation of the stratospheric winds over the tropics. *Journal of the Atmospheric Sciences*, *43*(17), 1873–1877. https://doi.org/10.1175/1520-0469(1986) 043<1873:AUOTOQ>2.0.CO;2

Park, J., Lühr, H., Kunze, M., Fejer, B. G., & Min, K. W. (2012). Effect of sudden stratospheric warming on lunar tidal modulation of the equatorial electrojet. *Journal of Geophysical Research*, *117*, A03306. https://doi.org/10.1029/2011JA017351

Scherhag, R. (1952). Die explosionsartigen Stratosphärenerwärmungen des Spätwinters 1951–1952. *Berichte der Deutschen Wetterdienstes*, *6*, 51–63.

Siddiqui, T. A., Stolle, C., Lühr, H., & Matzka, J. (2015). On the relationship between weakening of the northern polar vortex and the lunar tidal amplification in the equatorial electrojet. *Journal of Geophysical Research: Space Physics*, *120*, 10,006–10,019. https://doi.org/10.1002/2015JA021683

Stening, R. J. (1975). Problems of identifying lunar geomagnetic effects at Huancayo. *Journal of Geomagnetism and Geoelectricity*, *27*(5), 409–424. https://doi.org/10.5636/jgg.27.409

Stening, R. J., Forbes, J. M., Hagan, M. E., & Richmond, A. D. (1997). Experiments with a lunar atmospheric tidal model. *Journal of Geophysical Research: Atmospheres*, *102*(D12), 13,465–13,471. https://doi.org/10.1029/97JD00778

Tapping, K. F. (2013). The 10.7 cm solar radio flux (F10.7). *Space Weather*, *11*, 394–406. https://doi.org/10.1002/swe.20064

Vineeth, C., Kumar Pant, T., & Sridharan, R. (2009). Equatorial counter electrojets and polar stratospheric sudden warmings—A classical example of high latitude-low latitude coupling? *Annales Geophysicae*, *27*(8), 3147–3153. https://doi.org/10.5194/angeo-27-3147-2009

Yamazaki, Y., Richmond, A. D., & Yumoto, K. (2012). Stratospheric warmings and the geomagnetic lunar tide: 1958–2007. *Journal of Geophysical Research*, *117*, A04301. https://doi.org/10.1029/2012JA017514

Yamazaki, Y., Stolle, C., Matzka, J., Siddiqui, T. A., Lühr, H., & Alken, P. (2017). Longitudinal variation of the lunar tide in the equatorial electrojet. *Journal of Geophysical Research: Space Physics*, *122*, 12,445–12,463. https://doi.org/10.1002/2017JA024601